Published in AJSE, Vol: 25, Issue:1
Received on 15th May 2025
Revised on 19th August 2026
Published on 31st August 2026

AIUB JOURNAL OF SCIENCE AND ENGINEERING
ISSN: 1608 - 3679 (print) 2520 - 4890 (Online)
https://doi.org/10.53799/qgfg4692

Modified Chaotic Harris Hawks Optimization-Based PID Control for Load Frequency Control in Multi-Area Power System with Renewable Energy Integration

Sazzad Hossain Sahed, Kazi Firoz Ahmed and Md. Rifat Hazari

Abstract— **This research visions a Modified Chaotic Harris Hawks Optimization (MCHHO) algorithm for a three-area interconnected system comprising wind, solar and reheat thermal units to optimally tune a Proportional-Integral-Derivative (PID) controller with Integral of Time-weighted Absolute Error (ITAE) criterion for load frequency control (LFC). MCHHO incorporates consolidated strategies with chaotic map structure for enhancing exploration–exploitation balance and accelerating convergence. Results showcase a minimum ITAE of 0.0054 along with frequency and power settling within 3.8 s and 7 s, respectively. Comparative analysis with baseline algorithms, including BSA-PID, CLPSO-PID, MFOA-PID, OOA-PID and HHO-PID, displays performance improvement by 88.63%, 95.43%, 99.80%, 92.44% and 96.84%, respectively. Besides, robustness is validated under varied load disturbances, communication delays, renewable intermittencies and parametric uncertainties demonstrating the reliability and effectiveness of MCHHO in advanced LFC applications in interconnected power systems.**

Index Terms—**Modified Chaotic Harris Hawks Optimization (MCHHO), Three-area interconnected system, Proportional-Integral-Derivative controller, Integral of Time-weighted Absolute Error, Load frequency control, Consolidated strategies, chaotic map structure**

I. Introduction

Grids of the present and future solely operate as interconnected system consisting of renewable and conventional sources rather than isolated systems. It is challenging for such systems due to high unpredictability and cascaded power maintenance across areas. The operational framework of the interconnected system has been vastly transformed by the increasing renewable energy penetration. Despite the overall sustainability of such integration, some major challenges are still present in terms of frequency and power flow stability owing to the intermittent nature of renewable sources and complex power exchanges across interconnected regions.

Sazzad Hossain Sahed is pursuing M.Sc. degree in the Department of Electrical and Electronic Engineering and serves as a Graduate Teaching Assistant at American International University (AIUB). Email: 24-93424-2@student.aiub.edu

Kazi Firoz Ahmed serves as an Associate Professor in the Department of Electrical and Electronic Engineering at American International University (AIUB). Email: k.firoz@aiub.edu

Md. Rifat Hazari serves as an Associate Professor and Special Assistant in the Department of Electrical and Electronic Engineering at American International University (AIUB). Email: rifat@aiub.edu

Hence, Load Frequency Control (LFC) has emerged as a conducive response for preserving power system stability across various scenarios. Therefore, this work proposes a Modified Chaotic Harris Hawks Optimization (MCHHO)-based PID control strategy consolidating multiple exploitation behaviors into two unified update rules under a 1% SLP for a three-area power system comprising wind, reheat-thermal and solar unit. The key emphasize of this article is to evaluate the effectiveness of the proposed algorithm in tuning controller parameters leading to the deliberate adoption of PID controller due to its lower computational burden and structural complexity ensuring fair assessment of the strategy; rather than advanced fractional order or two-degree-of-freedom PID controllers.

The core contributions of this paper are followed by:

1. The sluggish dynamics of a conventional unit and the unstable nature of renewable sources are developed imitating a realistic and rigorous test environment.
2. A modified version of the Chaotic Harris Hawks Optimization algorithm (MCHHO) is introduced providing computational efficiency by reformulating canonical exploitation phases through unified update strategies and logistic chaotic map addition which replaces canonical random variables enhancing exploration–exploitation balance and replicability.

The rest of this paper follows chronological sequence: Section II highlights the previous works which dealt with multi-region based LFC applications and the associated research gaps. Section III illustrates the mathematical modeling and key components of the investigated three-area LFC system. Section IV outlines the controller structure, objective function and applied performance assessment criteria. The proposed Modified Chaotic Harris Hawk Optimization (MCHHO) algorithm is introduced in Section V. In Section VI, the comprehensive simulation findings along with comparative evaluation against other algorithms are provided. Furthermore, various test scenarios are utilized for the validity of the suggested strategy. Finally, Section VII concludes the research.

II. Literature Review

A. Related Works

Due to Load Frequency control (LFC) being one of the fundamental ancillary services in interconnected power systems, controllers such as PID have been utilized the most in multi-area systems due to simplicity in structure and satisfactory performance over the years housing both renewable and conventional sources [1, 2]. Challenging stability analysis, high tuning difficulty along with overall complexity and befuddling nature of the system led to the integration of simpler PI/PID controller setup with assistance from Backtracking Search Algorithm (BSA) [3] and Sea Horse Algorithm (SHA) [4]. Furthermore, PID controllers are also paired with advanced hybrid algorithms such as Hybrid Modified Artificial Bee Colony-Particle Swarm Optimization (MHABC-PSO) [5] and Hybrid Bald Eagle-Sparrow Search Optimization (BESSO) [6] for enhancing performance through complementary search capabilities. More recently, Harris Hawks Algorithm (HHO) has also been implemented for tackling sluggish dynamic response and poor disturbance rejection through [7, 8]. In addition to conventional controllers, it is also evident that the improved version of Harris Hawks Optimization Algorithm (EHHO) incorporating advanced controllers such as 3DOF-FOPIDN and 3DOF-TIDN are used for preserving power balance between source and load [9]. Additionally, modified controllers have been paired with metaheuristics (BA, MFO, GWO) [10–12], though they increase computational overhead. Consequently, improved single-algorithm variants have been preferred over hybrid multi-algorithms for PID-family tuning [13–16]. Due to improvement of population diversity and search space exploration, chaotic maps have been embedded in SCA [17] and ASO-TSA [18] to mitigate premature convergence leading to the proposed notion incorporating chaos.

B. Research Gaps

Such developments are crucial for the integration of chaos mechanism in stability analysis of renewable integrated multi-region load frequency control systems, however their applications in such scenario remains comparatively limited to some extent summarized in Table I.

TABLE I
A COMPREHENSIVE SUMMERY OF RECENT WORKS

Ref	Algorithm	Applications	Limitations
1	Gravitational Search Algorithm (GSA)	PID optimization for renewable integrated LFC	Limited test conditions and lacking range of operational complexities
2	Pelican Optimization Algorithm (POA)	PID optimization for renewable integrated LFC	High computational complexities requiring specialized monitoring
3	Backtracking Search Algorithm (BSA)	PI and PID optimization for renewable integrated LFC	Lack of wider variety of test conditions
4	Sea Horse Optimizer (SHO)	PI and PID optimization for renewable integrated LFC	Confined to simplified two-area system and possible local minima vulnerability
5	Hybrid: Modified Artificial Bee Colony-Particle Swarm Optimization (MHABC-PSO)	PID optimization for hybrid algorithm	Assumptions of the static operating conditions without varying dynamic loads
6	Hybrid: Bald Eagle-Sparrow Search Optimization (BESSO)	PID optimization for hybrid algorithm	Designed for linear system model resulting in incapability of handling large disturbances
7	Harris Hawks Optimization Algorithm (HHO)	TID optimization for single-area LFC	Confined to single-area system and limited test conditions
8	Harris Hawks Optimization Algorithm (HHO)	PID, FOPID and TID optimization for renewable integrated LFC	Confined to simplified two-area system under deregulated conditions
9	Enhanced Harris Hawks Optimization Algorithm (EHHO)	PID, 3DOF-FOPIDN and 3DOF-TIDN optimization for renewable integrated LFC	Complexity of advanced controllers leading to wider applicability
10	Bees Algorithm (BA)	Fuzzy cascaded controller optimization for LFC	Lacking renewable sources and additional fuzzy rules leading to longer execution time
11	Moth Flame Optimization (MFO)	PI-PDF optimization for renewable integrated LFC	Lacking automated tuning of parameters and limited test conditions
12	Grey Wolf Optimization (GWO)	PI-(1+DD) optimization for renewable integrated LFC	Confined to simplified two-area system
13	Modified Grey Wolf Optimization Algorithm and Cuckoo Search Algorithm (MGWO-CS)	TID optimization for renewable integrated LFC	Limited to two-area system and algorithm complexity leading to computational overhead
14	Modified Whale Optimization Algorithm (MWOA)	PIDF optimization for renewable integrated LFC	Algorithmic complexity and local optima entrapment
15	Improved Ant Colony Optimization (IACO)	FPID optimization for renewable integrated LFC	Increased computational overhead due to modified objective function
16	Optimized Grey Wolf Optimization (OGWO)	PID optimization for renewable integrated LFC	Despite algorithmic improvement, it faces local optimum phases
17	Chaotic Oppositional Sine–Cosine Algorithm (COSCA)	Global Optimization of non-linear optimization problems	Lacking investigation in high-dimensional engineering systems
18	Hybrid Chaotic Atom Search Optimization based on Tree-seed Algorithm (ASO-TSA)	Chaos based optimization	Large number of control mechanisms

A comparative analysis of the existing literature reveals various key research gaps which require proper addressing.

1. Most recent studies predominantly focus on simplified multi-region configurations. Particularly, three-area systems combining realistic configuration of wind, solar and reheat thermal are not comprehensively explored in recent optimization studies.
2. Recent advancements droop heavily on hybrid algorithms incorporated with complex controller architectures suffering from analytical complexity and minimal credibility.
3. Chaos-enhanced optimization strategies have demonstrated superb convergence capabilities, yet received limited investigation in renewable integrated three-area load frequency control problems.

III. Investigated System Model

The Simulink execution of the researched model depicted in Fig. 1 consists of three varied regions linked together in harmony where the framework houses both renewable (Wind and Solar) and conventional (Reheat Thermal). Area Control Error is integrated in this model acting as the core control signal for interconnected power systems [6].

$$ACE_i = B_i \Delta F_i + \sum_{i \neq j} \Delta P_{ij} \quad \text{for i=1,2,….N} \tag{1}$$

Where
B_i: Frequency bias coefficient
ΔF_i: Frequency divergence
ΔP_{ij}: Tie-line power flow divergence

The frequency bias coefficient for each area [6]

$$B_i = D_i + \frac{1}{R_i} \quad \text{for i=1,2,….N} \tag{2}$$

The power system [14]

$$G_{PS} = \frac{K_P}{1+T_P s} \tag{3}$$

The tie-line power flow across areas [2]

$$P_{ij} = \frac{|E_i||E_j|}{X_{ij}} \sin \delta_{ij} \quad \text{for i=1,2,….N} \tag{4}$$

A. Reheat Thermal Unit

The reheat thermal unit representing the conventional source serves as a major contributing unit where steam is sent to a reheater before it enters the low-pressure turbine [5]. The governor, turbine and reheater which control the unit are followed by [2, 14]

$$Governor = \frac{1}{1+T_G s} \tag{5}$$

$$Turbine = \frac{1}{1+T_T s} \tag{6}$$

$$Reheater = K_R \frac{1+T_{R1} s}{1+T_{R2} s} \tag{7}$$

B. Wind Power Unit

A blend of first-order lag denoting electrical response lag along with inherent converter delay and lead–lag compensator transfer functions defining aerodynamic turbine dynamics and rotor inertia is utilized [19]. The converter delay and rotor inertia are modeled by [20]

$$Converter\ Delay = \frac{1}{1+T_{W1} s} \tag{8}$$

$$Rotor\ Inertia = K_W \frac{1+T_{W2} s}{1+T_{W3} s} \tag{9}$$

C. Solar Power Unit

Likewise, the solar power unit in Area-3 is modeled with a combination of first-order lag and lead–lag compensator transfer functions imitating the dynamic behavior of inverter-based generation where the first-order lag corresponds to inverter's internal delay and the synthetic inertia is denoted by the lead-lag compensator [20].

$$Inverter\ Delay = \frac{1}{s+K_{PV1}} \tag{10}$$

Which can be algebraically normalized to the standard form

$$Inverter\ Delay = \frac{1}{1+T_{PV1} s} \tag{11}$$

The compact form is utilized for computational convenience, whereas the normalized version deals with clearer physical interpretation. The synthetic inertia can be modeled as

$$Synthetic\ Inertia = K_{PV2} \frac{1+T_{PV2} s}{1+T_{PV3} s} \tag{12}$$

The parameter values considered in Table II are within ranges reported in the literature representing realistic dynamic behavior of renewable and non-renewable units.

TABLE II
NOMINAL VALUES OF THE POWER SYSTEM

Parameters	Values	References
f	60 Hz	[3]
B_1=B_2=B_3	0.432 p.u.MW/Hz	[20]
R_1= R_2= R_3	2.4 Hz/p.u.MW	[1]
P_{R1}= P_{R2}= P_{R3}	1000 MW	[1]
$2\pi T_{12}$=$2\pi T_{23}$=$2\pi T_{13}$	0.545	[14]
T_{W1}	0.041 s	[20]
T_{W2}	0.6 s	[20]
T_{W3}	1 s	[20]
K_W	1.25	[20]
T_G	0.08 s	[15]
T_T	0.3 s	[15]
T_{R1}	5 s	[11]
T_{R2}	10 s	[11]
K_R	1	[11]
K_{PV1}=K_{PV2}	0.502525	[20]
T_{PV2}	0.02 s	[20]
T_{PV3}	0.01005 s	[20]
K_P	120 Hz/p.u.MW	[4]
T_P	20 s	[4]

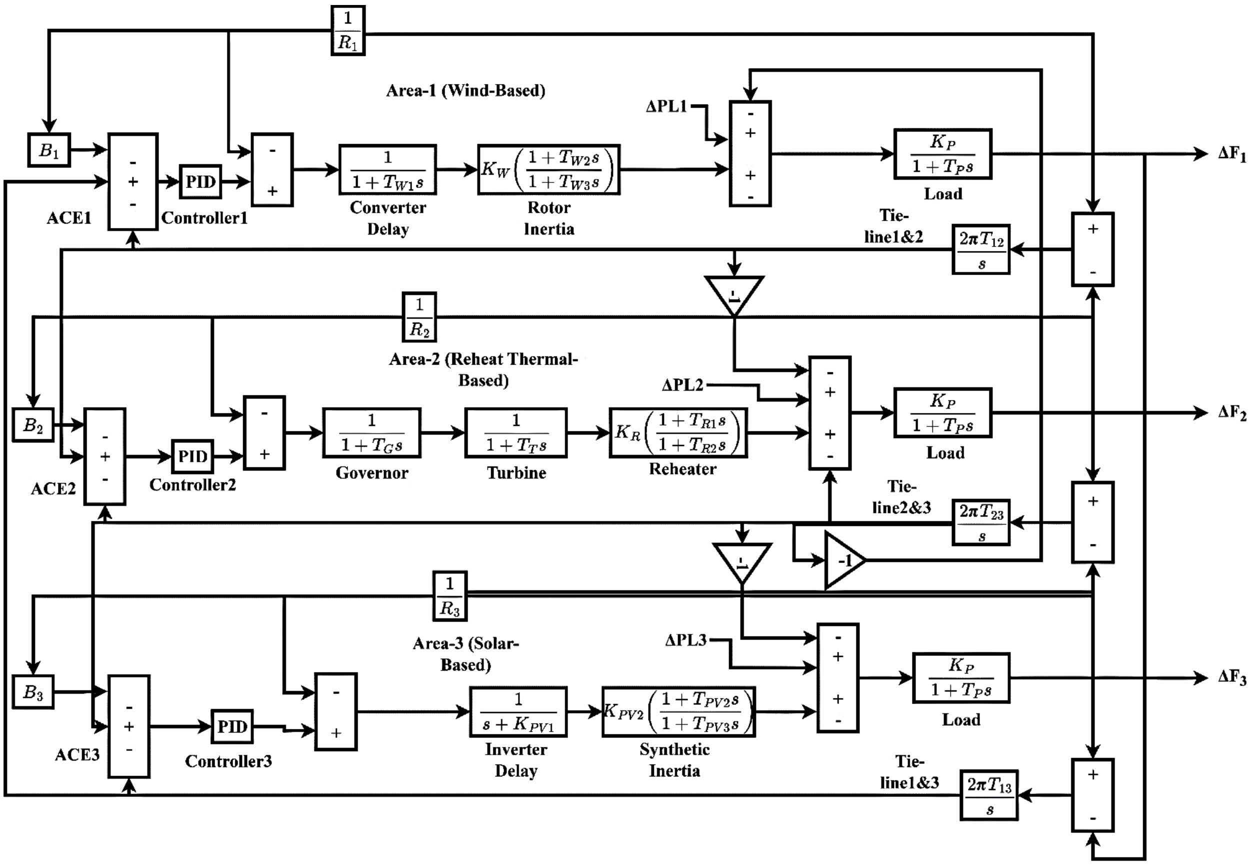

Fig. 1. Simulink Execution of the researched model

IV. Controller Approach

A. PID Controller

For multi-region system a controller is required whose aim is to attend desired state with minimal fluctuation [6]. PID controllers have well-established design methodology supported by straightforwardness, robustness, and satisfactory performance. The basic PID control arrangement is presented in Fig. 2 and Eq. (13).

$$G_{PID} = K_P + \frac{K_I}{s} + K_D s \tag{13}$$

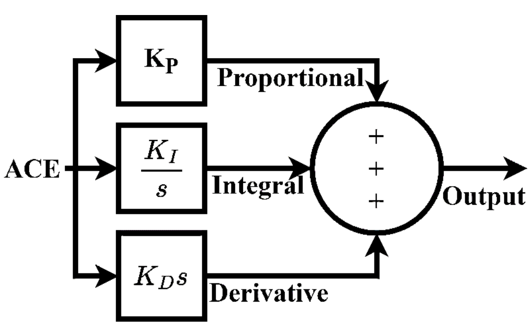

Fig. 2. Block diagram of Conventional PID Control

The output expression of the PID [6]

$$u(t) = K_P e(t) + K_I \int e(t)dt + K_D \frac{de(t)}{dt} \tag{14}$$

B. Objective Function

The controller gains are not selected arbitrarily, rather through effective performance criterion which ensures robust and satisfactory response [4]. Therefore, a fitness function is considered where steady-state and transient characteristics go through a trade-off [6].

$$ITAE = \int_0^{t_{sim}} (|\Delta F_1| + |\Delta F_2| + |\Delta F_3| + |\Delta P_{12}| + |\Delta P_{23}| + |\Delta P_{13}|)\, t\, dt \tag{15}$$

Where

t_{sim}: Maximum simulation time

ΔF_1=ΔF_2=ΔF_3: Frequency deviations across areas

ΔP_{12}=ΔP_{23}=ΔP13: Tie-line power deviations across areas

C. Performance Assessment Criteria

For incorporating the feasibility of the proposed strategy, multiple performance assessment criteria are considered consisting of robustness, communication delay, renewable intermittency and parameter sensitivity analyses.

Robustness refers to the disturbance rejection capability of the proposed strategy while maintaining acceptable frequency and tie-line power deviations evaluated through application of various single-area and multi-area step load perturbation scenarios. The applied SLP can be presented by Eq. (16).

$$\Delta P_L(t) = \sum_{i=1}^{N} \alpha_i u(t - t_i) \tag{16}$$

Where
ΔP_L: Total load perturbation
N: Number of disturbance locations
α_i: Applied disturbance
u(t): Unit step function

Communication delay analysis presents the capability of the proposed strategy to perform under delayed control action evaluated through incorporating deterministic transport delays and actuator nonlinearities by introducing both symmetrical and asymmetrical delay scenarios. The time delay can be presented by Eq. (17).

$$u_d(t) = u(t - \tau) \quad (17)$$

Where
$u_d(t)$: Delayed control signal
u(t): Original control signal
τ: Communication delay

Renewable Intermittency analysis displays feasibility of the suggested MCHHO strategy in maintaining satisfactory frequency regulation performance under intermittent renewable energy variations incorporating stochastic renewable generation profiles. The renewable power generation is presented by Eq. (18).

$$P_R(t) = P_N + \Delta P_W(t) + \Delta P_{PV}(t) \quad (18)$$

Where
$P_R(t)$: Instantaneous renewable power
P_N: Nominal renewable power
$\Delta P_W(t)$: Wind power fluctuation
$\Delta P_{PV}(t)$: Solar power fluctuation

Sensitivity analysis refers to the assessment of the proposed MCHHO strategy in sustaining nominal frequency and tie-line power flow under some distinct governing parameter uncertainties of the power system model. The parameter variation can be presented in Eq. (19).

$$\theta_i^{'} = \theta_i(1 + \delta) \quad (19)$$

Where
θ'_i: Perturbed parameter
θ_i: Nominal value of parameter
δ: Applied percentage variation

Hence, the feasibility of the proposed strategy is analyzed through varied load disturbances and parametric uncertainties where changes in parameters influence damping coefficient and system inertia of LFC. Moreover, load disturbances are related to generation-demand balance of LFC. Renewable intermittency referring to stochastic nature of renewable sources and communication delay referring to finite time required to transfer control signal are also crucial for LFC as they provide continues disturbances and reduce system stability.

V. Optimization Technique

Harris Hawks Optimization (HHO) has gained significance owing to maintaining equilibrium between exploration and exploitation phases supplemented by the Harris hawk's poaching tactics where they wait, observe and investigate the whereabouts of the target which may not always be readily present. The algorithm commences with the initialization of population of N hawks presented in Eq. (20) representing a candidate solution each.

$$X(i) = lb + rand(1, dim)\ (ub - lb) \quad (20)$$

A. Energy-Based Transition Mechanism

The escape energy of the target governs the shift from exploration to exploitation phases in HHO presented in Eq. (21).

$$E = E_1\, E_0 \quad (21)$$
$$E_1 = 2(1 - \frac{t}{Max_{iter}}) \quad (22)$$
$$E_0 = 2z - 1 \quad (23)$$

Here, stochastic or chaotic variation is introduced by E_0 where z is a chaotic variable and fatigue in the prey(rabbit) is stimulated by E_1.

Exploration phase continues if,
$|E| \geq 1$:

Exploitation phase commences if,
$|E| < 1$:

B. Exploration Phase

This chaos driven global search is responsible to ensure diversity in search trajectory and avoidance of local optima by utilizing two distinct strategies by the hawks for perching and monitoring the search [9].

Strategy 1: Position of other family members

Strategy 2: Position of the target

These two cases are visualized by using a mathematical model featured in Eq. (24) and Eq. (25).

$$if\ q < 0.5$$
$$X_{new} = X_{rand} - z\,|X_{rand} - 2z(X(i,:)) \quad (24)$$
$$if\ q \geq 0.5$$
$$X_{new} = \left(bestPos - mean(X)\right) - z\left((ub - lb)\,rand(1, dim)\ + lb\right) \quad (25)$$

C. Modified Chaotic HHO(MCHHO) Formulation

A modified chaotic variant is adopted to the existing algorithm which eliminates individual update rules related to redundant stochastic strategies like Lévy flight-based operators and consolidates multiple exploitation behaviors into two unified position update formulation. This modification avoids direct omission of conditions ensuring no loss of search diversity along with controlled perturbation. The search basis of the canonical HHO algorithm can be constructed through logistic chaotic maps and premature maturation is halted by such tweaks [21]. The updated chaotic variable is

$$z = 4z(1 - z) \tag{26}$$

D. Exploitation Phase

The exploitation phase mimics the attacking strategies of hawks incorporated by escape energy and escape probability using intensified capture mechanism and consolidated mechanism.

The Intensified Capture Mechanism (Escape Energy E < 0.5 and Escape Probability r ≥ 0.5) delineates the target becoming fatigued due to excessive chasing sequence by the predators by shrinking the distance between them leading to the commencement of the predator's surprise attack [21] modeled by the following Eq. (27).

$$X_{new} = bestPos - E\,|bestPos - X(i,:)| \tag{27}$$

The Consolidated Mechanism complies with the remaining conditions without revoking multiple strategies and acting upon a single, unified encirclement process where the prey still retains fractional escaping tendency through irregular motions and the predator aims to maintain controlled pursuit visualized by the adaptive jump strength of the prey denoted by J.

$$X_{new} = bestPos - E\,|J\,bestPos - X(i,:)| \tag{28}$$
$$J = 2\,(1 - z) \tag{29}$$

E. Workflow Structure

The procedural workflow of the MCHHO algorithm provided in Fig. 3 is a structured iterative optimization process integrated with chaotic dynamics and a consolidated exploitation structure. Furthermore, for reproducibility and implementation-level clarity, the step-by-step algorithm flow of the proposed scheme is summarized in Fig. 4.

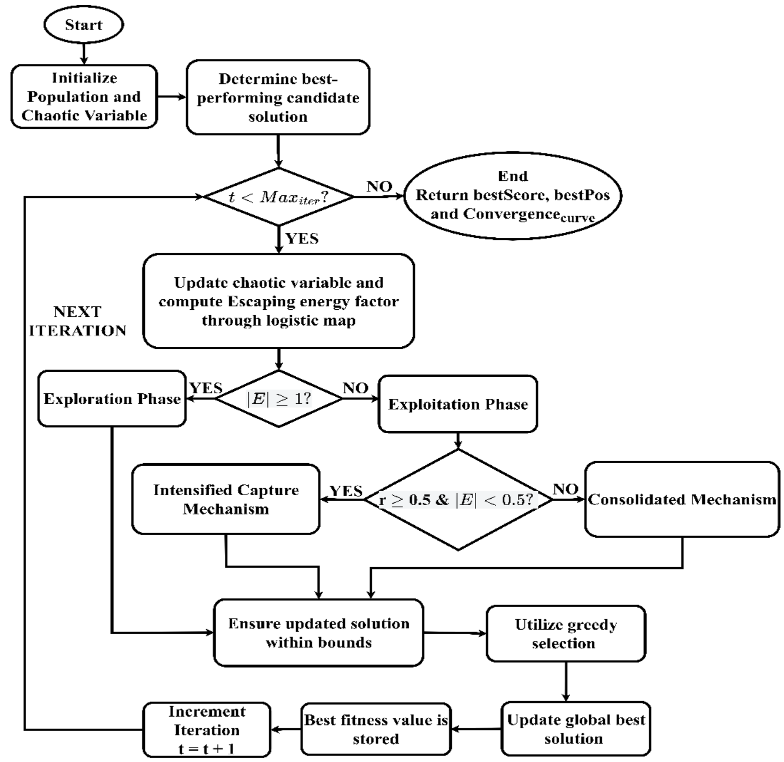

Fig. 3. Flowchart of MCHHO

Inputs: N (population size), Max_{iter} (maximum iterations), lb, ub (bounds), dim (dimension)
Outputs: bestScore (optimal ITAE), bestPos (optimal gains), $Convergence_{curve}$ (convergence history)
Initialize population X within bounds
Initialize chaotic variable z
Evaluate fitness of all hawks
Determine global best solution
For t = 1 to Max_{iter}
Compute escaping energy by Eq. (21)
Compute E_1 and E_0 by Eq. (22) and Eq. (23)
For each hawk i = 1 to N
Update chaotic variable by Eq. (26)
If |E| ≥ 1 %Exploration Phase
Random hawk selected
If q < 0.5 Compute X_{new} by Eq. (24)
Else Compute X_{new} by Eq. (25)
Else %Exploitation Phase
If |E| < 0.5 & r ≥ 0.5 %Intensified Capture Mechanism
Compute X_{new} by Eq. (27)
Else %Consolidated Mechanism
Compute X_{new} by Eq. (28)
Compute Jump Strength J by Eq. (29)
Apply bounds
Evaluate updated fitness
Update global best
Store Convergence history
Return bestScore, bestPos, $Convergence_{curve}$

Fig. 4. MCHHO Pseudocode

VI. Result Analysis

To vindicate the baseline feasibility of the proposed strategy, a three-area power system comprising wind, reheat thermal and solar sources is studied where a step load perturbation (SLP) of 1% in wind-based region is applied. Operational constraints are accepted to analyze the system performance where frequency deviation is limited within ±0.3 Hz, tie-line power flow deviations within ±0.8 MW along with a tolerance band of ±1% for settling time. Fig. 5, Fig. 6 and corresponding Table III states the frequency and power flow divergence across all areas considered.

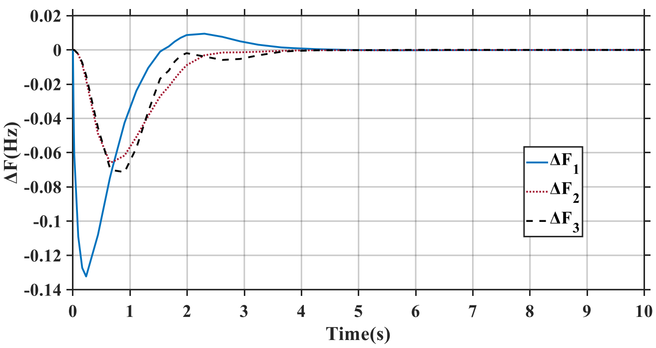

Fig. 5. Baseline deviations in frequency across three areas

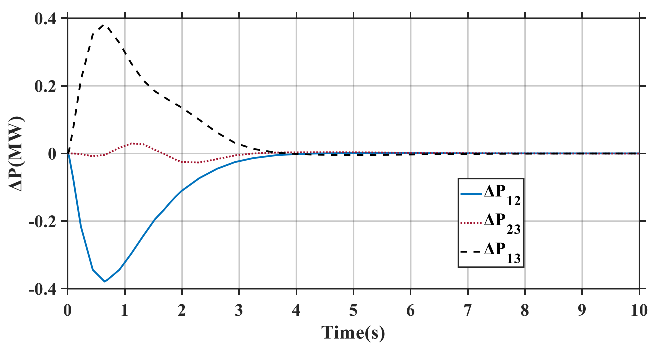

Fig. 6. Baseline deviations in power across three areas

TABLE III
BASELINE PERFORMANCE INDICES OF FREQUENCY AND TIE-LINE POWER FLOW DEVIATIONS ACROSS THREE AREAS

P	ΔF_1	ΔF_2	ΔF_3	ΔP_{12}	ΔP_{23}	ΔP_{13}
T_s	3.846	3.2445	3.6445	5.8545	6.6545	7.0545
OS	0.0094	0	0.00003	0.0012	0.0296	0.38296
US	-0.1323	-0.065	-0.0714	-0.378	-0.026	-0.0044

A. *Comparative Analysis*

The statistical performance and convergence behavior of canonical HHO, chaotic HHO and MCHHO is provided in Table IV and Fig. 7 where in terms of mean ITAE, proposed MCHHO achieved the lowest value of 0.0054113 superior to HHO and CHHO by 15.57% and 10.89% respectively over 20 independent runs. Furthermore, the proposed MCHHO also achieved the smallest standard deviation of 0.000177 exhibiting a reduction of around 48% compared to HHO and CHHO. Such results showcase that, MCHHO is more consistent and robust across multiple runs. Besides, MCHHO also achieved lowest minimum ITAE and maximum ITAE value. Additionally, the convergence behavior of the methods reveals that, despite MCHHO reaching competitive ITAE value over a single run, it reaches near optimum value within 3rd iteration with minor refinement at later iterations due to chaotic perturbation which continues to maintain exploratory motion for adjusting accuracy even after achieving stability. In addition, this post stability refinement doesn't lead to destabilizing the system; instead, it ensures adaptive fine-search capability exhibiting the efficiency of the algorithm towards sustaining convergence accuracy. Now, for HHO and CHHO the convergence behavior shows a much larger variation in convergence profile leading to the overall superior optimization effectiveness of MCHHO over canonical HHO and its chaotic variation based on various performance criterion.

TABLE IV
STATISTICAL COMPARISON OF MCHHO, CHHO AND HHO OVER MULTIPLE RUNS

Algorithm	Best ITAE	Mean ITAE	Worst ITAE	Standard Deviation
MCHHO	0.005008	0.0054113	0.005924	0.000177
CHHO	0.005311	0.0060726	0.006729	0.000339
HHO	0.005872	0.0064094	0.006958	0.000338

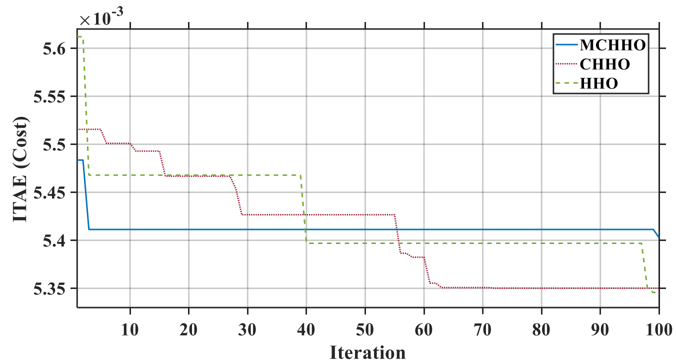

Fig. 7. Convergence characteristics of MCHHO, CHHO and HHO

Table V demonstrates the comprehensive comparative performance analysis of the proposed MCHHO-PID strategy over myriad existing optimization techniques for three-area LFC system based on renewable and conventional sources with an identical operating condition of 1% disturbance in Area-1. Other than MCHHO, the near best-performing existing method (OOA-PID) [22] yields a frequency settling time of 4 s, 5.5 s, and 6 s across the three areas respectively governing an increase of approximately 4%, 69% and 65% in contrast to MCHHO.

In terms of overshoot, minimal oscillatory behavior is witnessed for the proposed MCHHO-PID controller with an elimination of 100% overshoot in Area-2 (Reheat Thermal-based) and negligible amount in other corresponding areas with an exceptional reduction of around 73% in Area-3 (Solar-based) compared to the near best OOA-PID controller. Although, a slightly higher overshoot is observed in Area-1 compared to other existing algorithms, it still remains within the acceptable limits damping effectively in shorter duration. The optimized PID gains derived from MCHHO algorithm against other conventional strategies are provided in Table VI which serve as the basis for dynamic performance evaluation across all the optimization techniques and Table VII quantifies the

ITAE improvement, ranging from 88.63% (BSA) to 99.80% (MFOA)Hence, despite unification of exploitation mechanisms, the proposed MCHHO-PID strategy assures faster settling time, minimal oscillations and low objective function compared to other benchmark algorithms, establishing strong computational efficiency which indicates a successful compensation for the proposed consolidation.

TABLE V
COMPARATIVE ANALYSIS AMONG VARIOUS BASELINE OPTIMIZATION TECHNIQUES IN TERMS OF SETTLING TIMES, OVERSHOOTS AND ITAE VALUES

Methods	T_S(s)			Overshoot (Hz)			ITAE
	ΔF_1	ΔF_2	ΔF_3	OS_1	OS_2	OS_3	
BSA-PID [3]	8.68	25.8	29.7	0.002	0.0021	0.0044	0.0475
CLPSO-PID [3]	16.37	17.03	17.77	0.0092	0.0049	0.0053	0.1181
MFOA-PID [11]	61.42	31.53	29.13	0.0067	0.0041	0.0042	2.7912
OOA-PID [22]	4	5.5	6	**0.0005**	0.00035	0.00012	0.07142
HHO-PID [2]	8.8	7	8.8	0.022	0.0037	0.0021	0.17066
MCHHO-PID	**3.846**	**3.245**	**3.645**	0.009457	**0**	**0.000032**	**0.0054**

TABLE VI
OPTIMIZED PID GAINS OF MYRIAD OPTIMIZATION TECHNIQUES

Algorithms	Area-1			Area-2			Area-3		
	K_{P1}	K_{I1}	K_{D1}	K_{P2}	K_{I2}	K_{D2}	K_{P3}	K_{I3}	K_{D3}
BSA-PID [3]	1.9667	0.8788	0.0116	1.881	0.0265	0.0622	1.0067	1.9784	0.1919
CLPSO-PID [3]	0.9533	0.979	0.3341	0.8919	0.9867	0.3114	0.7488	0.4464	0.6467
MFOA-PID [11]	-0.5	0.0113	0.1352	0.3508	-0.4999	0.3046	0.1933	-0.2141	-0.4737
OOA-PID [22]	9.9614	0.6459	9.4983	10	9.9964	9.6198	0.6795	4.6792	10
HHO-PID [2]	10	8.329	7.238	5.768	8.069	8.927	-3.893	0.402	-0.892
MCHHO-PID	**5**	**4.9986**	**0.9932**	**10**	**10**	**0.8293**	**6**	**6**	**0.9988**

TABLE VII
IMPROVEMENT OF ITAE OVER VARIOUS OPTIMIZATION TECHNIQUES

Methods	ITAE Improvement of **MCHHO-PID**
BSA-PID [3]	88.63%
CLPSO-PID [3]	95.43%
MFOA-PID [11]	99.80%
OOA-PID [22]	92.44%
HHO-PID [2]	96.84%

B. Robustness Analysis

For incorporating the behavior of the proposed PID based MCHHO algorithm, diverse load demands were brought into the equation for ensuring feasibility in terms of system robustness [23]. Table VIII and Table IX summarizes performance done through altering the step load perturbations (SLP) involving single and multi-area disturbances. Additionally, Fig. 8 and Fig. 9 illustrates the frequency and power flow deviations across all three areas where it is seen that the frequency responses in nominal case settle within 3.85 s compared to the second scenario settling within 3.93 s having negligible performance degradation and with the introduction of several multi-area disturbance it settles within 8.99 s which is 133.51% more than the nominal case being acceptable due to increased system stress. Similarly, the maximum undershoot of -0.28 Hz occurs in the in worst-case scenario in Area-1 remaining within predefined tolerance with negligible overshoot. Moreover, for power flow, the maximum undershoots and overshoot values also remain within preferred bounds and settles within 7.05 s for nominal case.

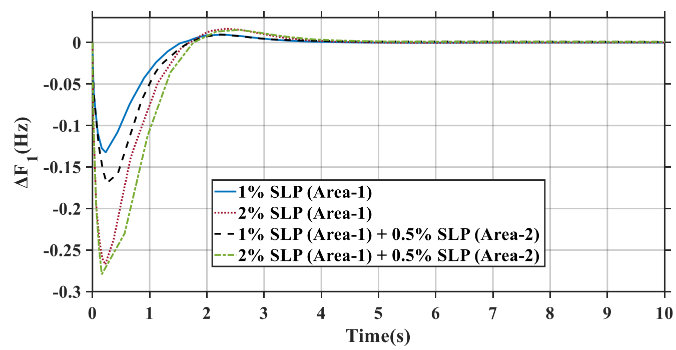

(a)

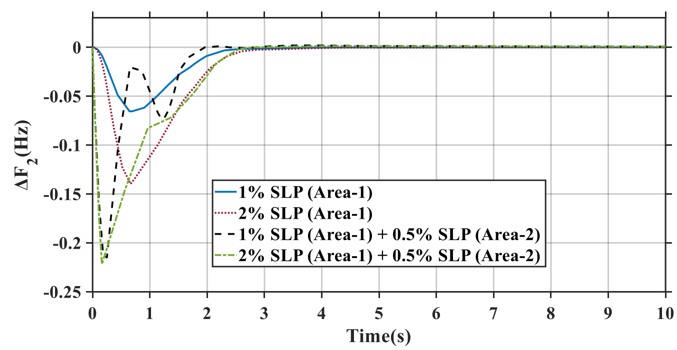

(b)

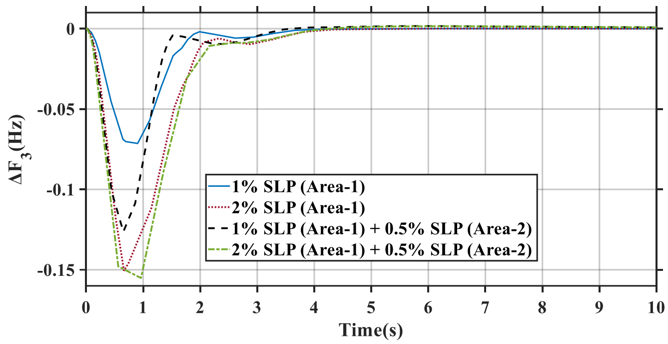

(c)

Fig. 8. Robustness Analysis considering deviations in frequency across three areas (a), (b) and (c)

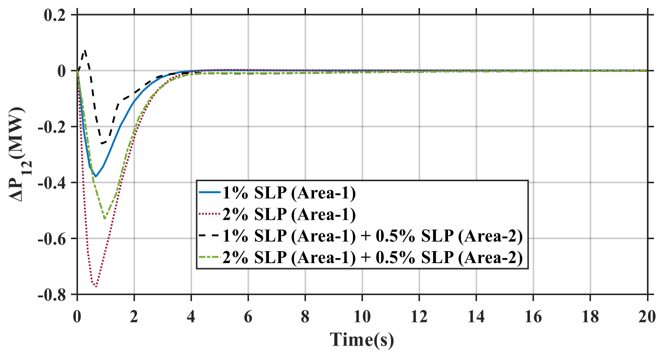

(a)

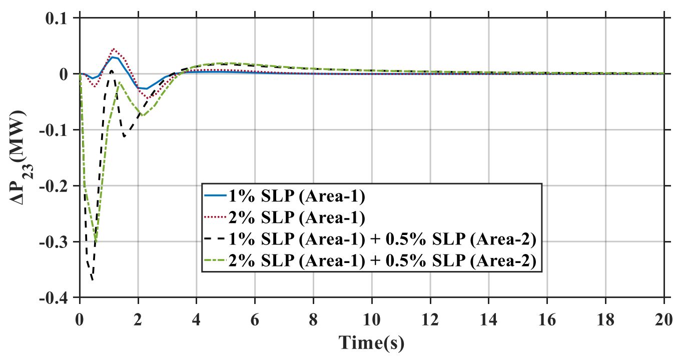

(b)

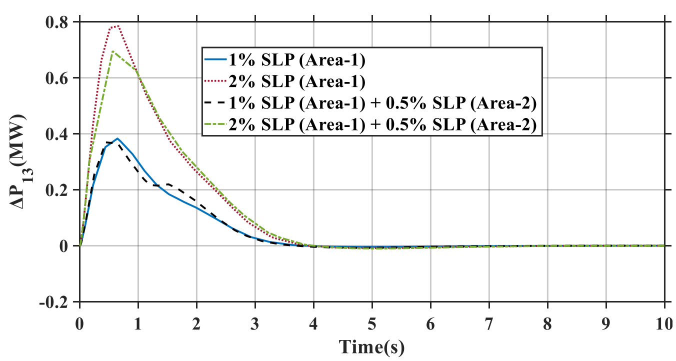

(c)

Fig. 9. Robustness Analysis considering deviations in power across three areas (a), (b) and (c)

TABLE VIII
SUMMARIZED ROBUSTNESS ANALYSIS CONSIDERING OS AND US

Delay Types		Nominal Case	2% SLP (Area-1)	1% SLP (Area-1) + 0.5% SLP (Area-2)	2% SLP (Area-1) + 0.5% SLP (Area-2)
ΔF_1	OS	0.0094	0.016626	0.009622	0.015248
	US	-0.1323	-0.267327	-0.169522	-0.279272
ΔF_2	OS	0	0	0.0019	0.001348
	US	-0.065	-0.139797	-0.215441	-0.221915
ΔF_3	OS	0.00003	0.000057	0.001637	0.001532
	US	-0.0714	-0.150628	-0.126332	-0.15517
ΔP_{12}	OS	0.0012	0.002324	0.078976	0
	US	-0.378	-0.772708	-0.261121	-0.530628
ΔP_{23}	OS	0.0296	0.04526	0.017118	0.018937
	US	-0.026	-0.04375	-0.369387	-0.301386
ΔP_{13}	OS	0.38296	0.784568	0.369387	0.695161
	US	-0.0044	-0.008568	-0.00735	-0.010039

TABLE IX
SUMMARIZED ROBUSTNESS ANALYSIS CONSIDERING SETTLING TIME

SLP	T_S(s)					
	ΔF_1	ΔF_2	ΔF_3	ΔP_{12}	ΔP_{23}	ΔP_{13}
1% SLP (Area-1) (Nominal Case)	3.846	3.2445	3.6445	5.8545	6.6545	7.0545
2% SLP (Area-1)	3.9327	3.7806	3.9327	6.7801	7.1801	7.5801
1% SLP (Area-1) + 0.5% SLP (Area-2)	8.5428	7.7428	8.9982	18.9982	18.5982	6.9428
2% SLP (Area-1) + 0.5% SLP (Area-2)	8.2626	7.0626	8.6626	18.7929	18.7929	7.8626

C. Communication Delay Analysis

The feasibility of the MCHHO-PID strategy is further proven through the introduction of communication delays and actuator nonlinearities in the model to capture non-ideal physical constraints under deterministic or fixed delay conditions due to its computationally tractable nature. As seen in Fig. 10 and Fig. 11 the nominal condition exhibits well-damped responses with rapid settling times well within the predefined tolerance. However, considering symmetrical delays the frequency settles within 4.99 s across the areas and within 5.5 s in case of uneven conditions indicating noticeable degradation marking an increment of 42.86% compared to the nominal case despite being within preferred bounds. Besides, both delay scenarios result in moderate to high fluctuation compared to the nominal scenario and increased maximum undershoot of -0.288 Hz evident in Area-1 nearly twice that of nominal case with insignificant overshoot. Similarly, power settles approximately within 7.33 s in comparison with 7.12 s in nominal case and due to inter-area power imbalance, experience large excursions especially in Area-1 and Area-3 with an undershoot and overshoot reaching -0.449 MW and 0.46 MW. Table X and Table XI summarize the performance based on several deterministic delay scenarios.

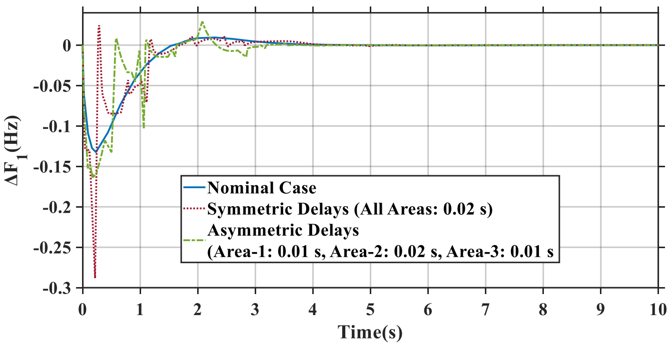

(a)

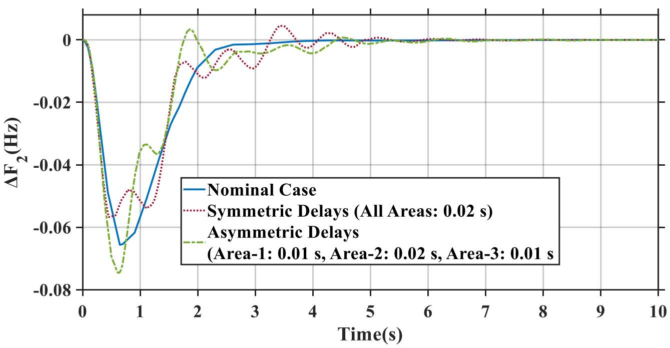

(b)

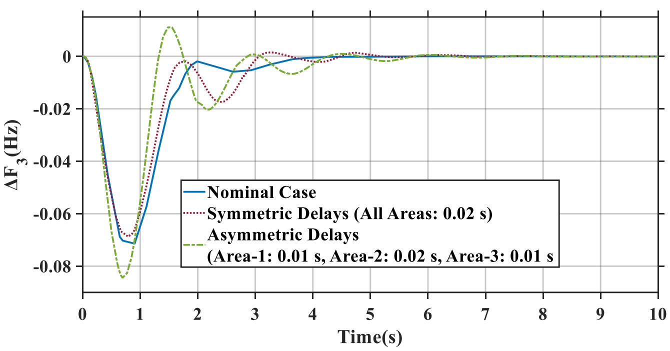

(c)

Fig. 10. Communication Delay Analysis considering deviations in frequency across three areas (a), (b) and (c)

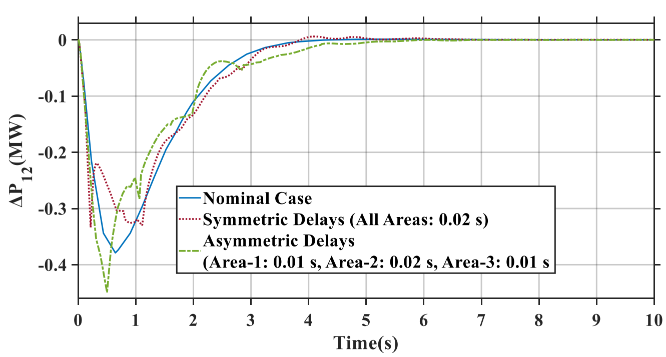

(a)

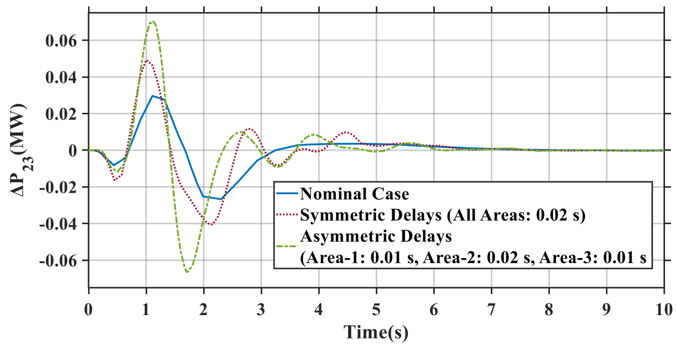

(b)

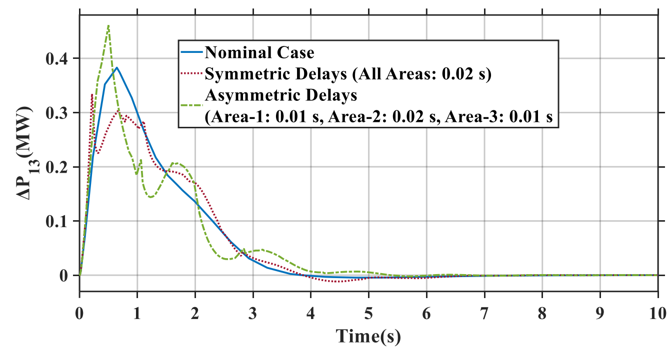

(c)

Fig. 11. Communication Delay Analysis considering deviations in power across three areas (a), (b) and (c)

TABLE X
SUMMARIZED COMMUNICATION DELAY ANALYSIS CONSIDERING OS AND US

Delay Types		Nominal Case	Symmetrical	Asymmetrical
ΔF_1	OS	0.0094	0.024433	0.028653
	US	-0.1323	-0.28827	-0.164005
ΔF_2	OS	0	0.004553	0.003444
	US	-0.065	-0.056739	-0.07458
ΔF_3	OS	0.00003	0.001471	0.011068
	US	-0.0714	-0.068719	-0.084444
ΔP_{12}	OS	0.0012	0.006041	0.000213
	US	-0.378	-0.333404	-0.449268
ΔP_{23}	OS	0.0296	0.049196	0.070146
	US	-0.026	-0.040512	-0.066586
ΔP_{13}	OS	0.38296	0.334521	0.461141
	US	-0.0044	-0.011614	-0.002039

TABLE XI
SUMMARIZED COMMUNICATION DELAY ANALYSIS CONSIDERING SETTLING TIME

Delay Types	T_S(s)					
	ΔF_1	ΔF_2	ΔF_3	ΔP_{12}	ΔP_{23}	ΔP_{13}
Nominal Case	3.846	3.2445	3.6445	5.8545	6.6545	7.0545
Symmetrical	4.9986	4.7358	4.7358	6.5842	6.3894	7.1235
Asymmetrical	3.5153	5.0965	5.5036	6.5698	7.3314	5.9543

D. Renewable Intermittency Analysis

Stochastic renewable generation profiles are incorporated to test the capability of the controller by means of the intermittent wind speed and solar irradiance. Fig. 12 displays the deviation of frequency where nominal condition exhibits fast stabilization compared to renewable intermittency scenarios settling within 7.8-8.8 s for standalone wind generation profile. Additionally, due to strong stochastic-heavy fluctuations by simultaneous wind and solar units, the frequency still settles within standard means despite slow stabilization. Fig. 13 also demonstrates that the power settles within bounds of 7. 068 s to around 20 s in case of multi sources intermittent scenario. Likewise, under both intermittent scenarios the frequency and power oscillate within predefined limits suppressed by the proposed strategy. Table XII and Table XIII summarizes the performance based on renewable profiles.

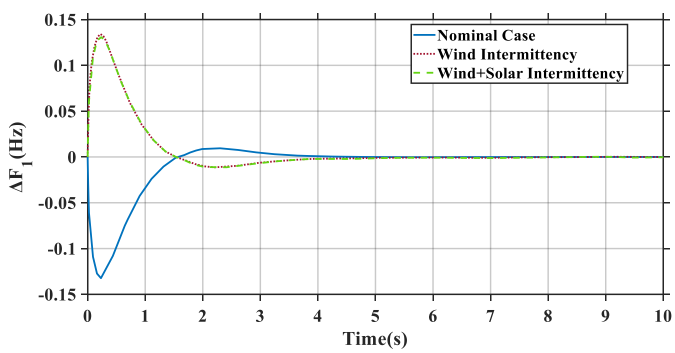

(a)

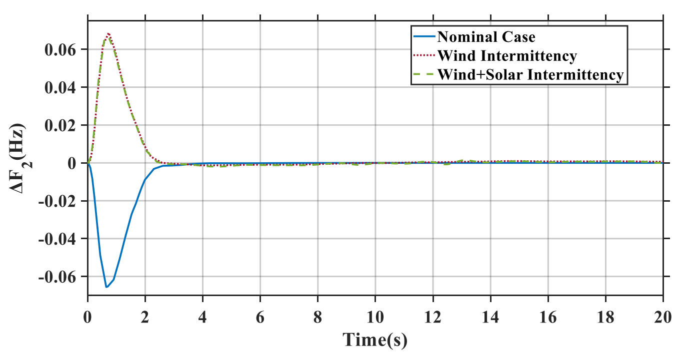

(b)

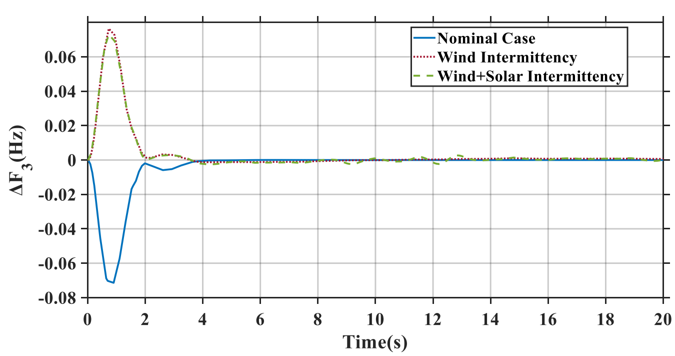

(c)

Fig. 12. Renewable Intermittency Analysis considering deviations in frequency across three areas (a), (b) and (c)

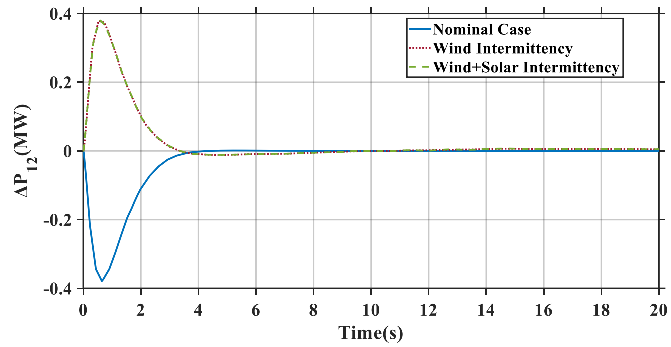

(a)

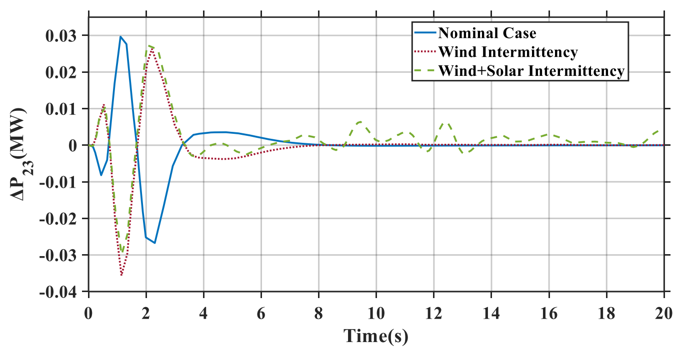

(b)

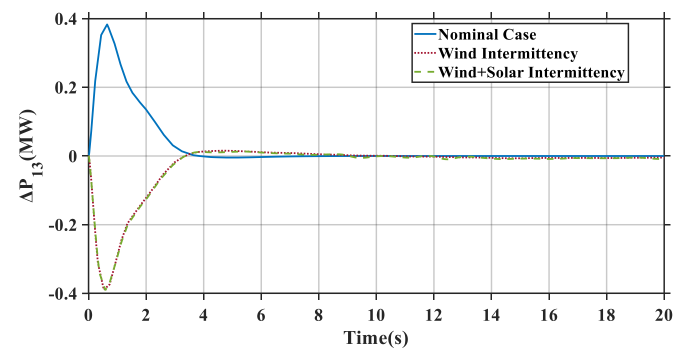

(c)

Fig. 13. Renewable Intermittency Analysis considering deviations in power across three areas (a), (b) and (c)

TABLE XII
SUMMARIZED RENEWABLE INTERMITTENCY ANALYSIS CONSIDERING OS AND US

Renewable Profiles		Nominal Case	Wind Intermittency	Wind + Solar Intermittency
ΔF_1	OS	0.0094	0.133438	0.130723
	US	-0.1323	-0.012043	-0.011425
ΔF_2	OS	0	0.068151	0.066358
	US	-0.065	-0.001962	-0.001972
ΔF_3	OS	0.00003	0.075793	0.072918
	US	-0.0714	-0.001915	-0.002740
ΔP_{12}	OS	0.0012	0.373447	0.375448
	US	-0.378	-0.016293	-0.016320

ΔP_{23}	OS	0.0296	0.026299	0.023403
	US	-0.026	-0.035623	-0.033867
ΔP_{13}	OS	0.38296	0.020127	0.021974
	US	-0.0044	-0.384568	-0.381967

TABLE XIII
SUMMARIZED RENEWABLE INTERMITTENCY ANALYSIS CONSIDERING SETTLING TIME

Renewable Profiles	T_S(s)					
	ΔF_1	ΔF_2	ΔF_3	ΔP_{12}	ΔP_{23}	ΔP_{13}
Nominal Case	3.846	3.2445	3.6445	5.8545	6.6545	7.0545
Wind Intermittency	7.868	8.802	8.802	18.958	7.068	18.558
Wind + Solar Intermittency	7.856	13.444	17.199	15.599	19.647	19.647

E. Sensitivity Analysis

Substantial fluctuations in key parameters from the model are applied to validate the controller's resilient capabilities and sensitivity of the proposed strategy with respect to the nominal response. Fig. 14 show that parametric variations (±25% T_G/T_R, ±50% K_P/T_P/P_S) only marginally affect settling time; the worst case (-50% P_S) increases settling time to 4.74 s (23.4% degradation), yet all trajectories remain within bounds. Additionally, Fig. 15 illustrates the power flow divergence where the power settles within close margin and oscillations remain within bounds approximately identical to the baseline. Table XIV and Table XV further provide the summarized dynamic performance of the LFC system

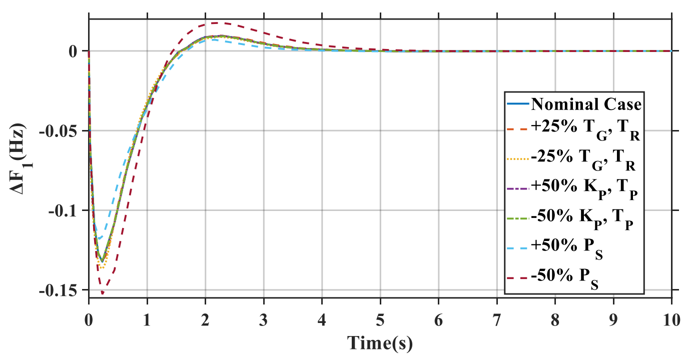

(a)

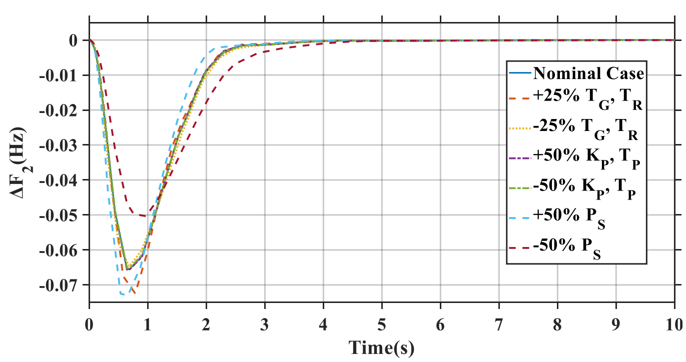

(b)

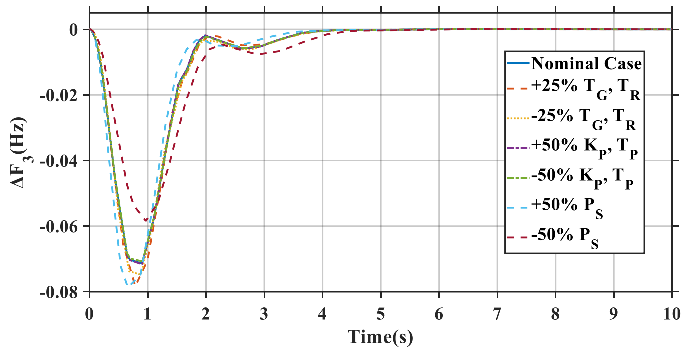

(c)

Fig. 14. Sensitivity Analysis considering deviations in frequency across three areas (a), (b) and (c)

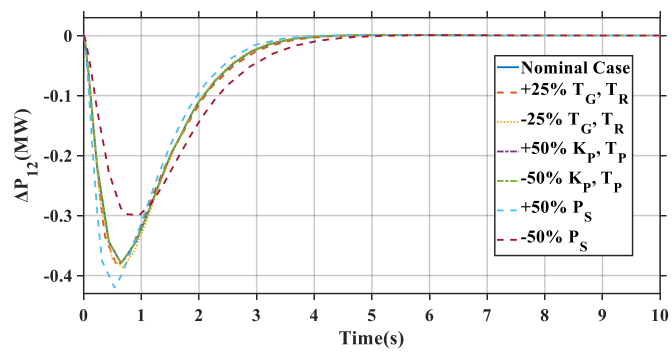

(a)

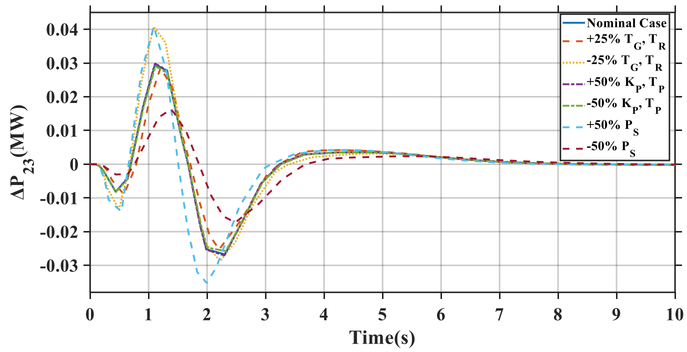

(b)

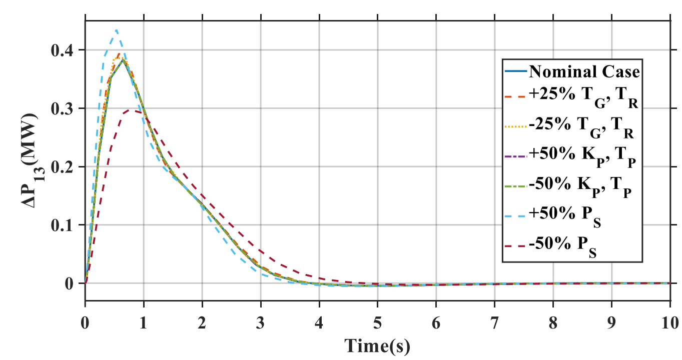

(c)

Fig. 15. Sensitivity Analysis considering deviations in power across three areas (a), (b) and (c)

TABLE XIV
SUMMARIZED SENSITIVITY ANALYSIS CONSIDERING OS AND US

Parameters		Nominal Case	+25% T_G, T_R	-25% T_G, T_R	+50% K_P, T_P	-50% K_P, T_P	+50% P_S	-50% P_S
ΔF_1	OS	0.0094	0.009857	0.008901	0.009539	0.009213	0.00702	0.017648
	US	-0.1323	-0.131695	-0.1365	-0.132405	-0.132083	-0.118058	-0.15268
ΔF_2	OS	0	0	0	0	0	0	0
	US	-0.065	-0.072455	-0.064724	-0.065709	-0.065237	-0.073036	-0.050336
ΔF_3	OS	0.00003	0.000032	0.000038	0.000032	0.000032	0	0.000099
	US	-0.0714	-0.078348	-0.074817	-0.071621	-0.070749	-0.078714	-0.058418
ΔP_{12}	OS	0.0012	0.001033	0.001454	0.001221	0.001238	0.00135	0.000788
	US	-0.378	-0.384841	-0.386304	-0.378911	-0.378875	-0.420526	-0.299172
ΔP_{23}	OS	0.0296	0.028523	0.040785	0.029864	0.029063	0.040867	0.016275
	US	-0.026	-0.025293	-0.028746	-0.027061	-0.025766	-0.035211	-0.017291
ΔP_{13}	OS	0.38296	0.393825	0.386304	0.382858	0.383258	0.434577	0.297826
	US	-0.0044	-0.004399	-0.004543	-0.004487	-0.004456	-0.005252	-0.00292

TABLE XV
SUMMARIZED SENSITIVITY ANALYSIS CONSIDERING SETTLING TIME

Parameters	T_S(s)					
	ΔF_1	ΔF_2	ΔF_3	ΔP_{12}	ΔP_{23}	ΔP_{13}
Nominal Case	3.846	3.2445	3.6445	5.8545	6.6545	7.0545
+25% T_G, T_R	3.8843	3.0061	3.628	5.5604	6.474	7.2002
-25% T_G, T_R	3.7959	3.1634	3.3959	5.8022	6.5135	6.8692
+50% K_P, T_P	3.8436	3.2375	3.6375	5.8516	6.6516	7.0516
-50% K_P, T_P	3.8533	3.2652	3.6652	5.8613	6.6613	7.0613
+50% P_S	3.0924	2.9555	3.0924	5.4856	6.2856	6.6856
-50% P_S	4.7394	3.677	4.077	4.7394	6.9638	7.7146

VII. CONCLUSION

The proposed work put forth a three-area renewable and conventional interconnected LFC unit combined with wind, reheat thermal and solar units. A conventional PID controller optimizes the divergence associated with frequency and tie-line power of the system analyzed through myriad realistic operating conditions tuned by MCHHO algorithm which integrates consolidated strategies and adaptive chaotic logistic map. The proposed algorithm significantly reduces the ITAE value to 0.0054, while ensuring the stabilization of frequency and power within 3.8 s and 7 s respectively across all three areas. Compared to other established techniques, including BSA-PID, CLPSO-PID, MFOA-PID, OOA-PID and HHO-PID, the MCHHO-PID showed an improved efficacy level in the margin of 88.63%, 95.43%, 99.80%, 92.44% and 96.84% accordingly certifying it's superiority. Besides, a rapid convergence within the early iterations is witnessed, reaching near optimal values exhibiting computational efficiency. Additionally, the findings based on multiple real-world system constraints demonstrated that the PID controller maintains tremendous resilience by oscillating within predefined standard bounds without increasing structural or computational complexities. Despite such advantages, certain limitations are acknowledged such as lack of further investigation in larger systems proving scalability and necessity of frequent retuning of linear PID structure under highly nonlinear and time-varying operating conditions. Future work aims to mitigate such drawbacks and extend the applicability of MCHHO-PID for multi-area LFC studies. A promising direction to improve feasibility is through testing the technique in broader array of power system with more diverse key uncertainties such as investigating stochastic realistic delay models along with integration of the algorithm with adaptive or nonlinear control strategies.

Author Contributions

Mr. Sazzad Hossain Sahed conducted the major research activities with assistance from Mr. Kazi Firoz Ahmed and Mr. Md. Rifat Hazari, including conceptualization, methodology development, analysis, interpretation of results, and manuscript preparation. Additionally, Mr. Kazi Firoz Ahmed provided academic supervision, research guidance and critical feedback as well. On the other hand, Mr. Md. Rifat Hazari provided additional academic and technical guidance with constructive feedback during the research development.

AI Tool Usage Acknowledgement

No generative AI tools were used in the coding, simulation, data analysis, or writing of this manuscript where all research activities and manuscript content were prepared independently by the authors.

REFERENCES

[1] S. J. Y. et al., "Gravitational search algorithm-basedautomatic load frequency control for multi-area interconnected power system," Turk. J. Comput. Math. Educ., vol. 12, no. 3, pp. 4548–4568, Apr. 2021, doi: 10.17762/turcomat. v12i3.1845.

[2] A. Shafee et al., "Techno-Economic Feasibility Analysis of Hybrid System in Bangladesh - A Case Study for Higher Learning Institution," 2023 3rd International Conference on Robotics, Electrical and Signal Processing Techniques (ICREST), Dhaka, Bangladesh, 2023, pp. 275-279, doi: 10.1109/ICREST57604.2023.10070053.

[3] D. Guha, P. K. Roy, and S. Banerjee, "Application of backtracking search algorithm in load frequency control of multi-area interconnected power system," Ain Shams Eng. J., vol. 9, no. 2, pp. 257–276, Feb. 2016, doi: 10.1016/j.asej.2016.01.004.

[4] C. Andic, S. Ozumcan, M. Varan, and A. Ozturk, "A novel sea horse optimizer-based load frequency controller for two-area power system with PV and thermal units," Int. J. Robot. Control Syst., vol. 4, no. 2, pp. 606–627, May 2024, doi: 10.31763/ijrcs. v4i2.1341.

[5] M. S. Iqbal, M. F. A. Limon, M. M. Kabir, M. K. M. Rabby, M. J. A. Soeb, and M. F. Jubayer, "A hybrid optimization algorithm for improving load frequency control in interconnected power

systems," Expert Syst. Appl., vol. 249, p. 123702, Mar. 2024, doi: 10.1016/j.eswa.2024.123702.

[6] T. D. Raj, C. Kumar, P. Kotsampopoulos, and H. H. Fayek, "Load frequency control in two-area multi-source power system using bald eagle–sparrow search optimization tuned PID controller," Energies, vol. 16, no. 4, p. 2014, Feb. 2023, doi: 10.3390/en16042014.

[7] M. M. Alrashed and M. F. Elnaggar, "An HHO-optimized TI–TD control strategy for enhancing microgrid frequency stability under renewable energy uncertainty," J. Robot. Control (JRC), vol. 6, no. 6, pp. 1957–1973, Nov. 2025, doi: 10.18196/jrc. v6i6.22359.

[8] A. Maji et al., "A comparative study of PID, FOPID, and TID controllers using Harris hawk's optimization for load frequency control of renewable energy grids in deregulated environments," in Proc. Int. Conf. Signal Process., Comput. Control (ISPCC), Mar. 2025, pp. 118–123, doi: 10.1109/ISPCC66872.2025.11039571.

[9] C. Rohmingtluanga et al., "Enhanced Harris hawks' optimization-based load frequency control of multi-area microgrid-based water treatment plant with consideration of 3DOF-(FO-PIDN)/(TIDN) controller," Front. Energy Res., vol. 12, Apr. 2024, doi: 10.3389/fenrg.2024.1387780.

[10] M. Shouran, F. Anayi, M. Packianather, and M. Habil, "Different fuzzy control configurations tuned by the BEES algorithm for LFC of two-area power system," Energies, vol. 15, no. 2, p. 657, Jan. 2022, doi: 10.3390/en15020657.

[11] B. V. S. Acharyulu, B. Mohanty, and P. K. Hota, "Analysis of moth flame optimization-optimized cascade proportional–integral–proportional–derivative controller with filter for automatic generation control system incorporating solar thermal power plant," Optim. Control Appl. Methods, vol. 41, no. 3, pp. 866–881, Feb. 2020, doi: 10.1002/oca.2582.

[12] O. Can, A. Ozturk, H. Eroğlu, and H. Kotb, "A novel grey wolf optimizer-based load frequency controller for renewable energy sources integrated thermal power systems," Electr. Power Compon. Syst., vol. 49, no. 15, pp. 1248–1259, Sep. 2021, doi:10.1080/15325008.2022.2050450.

[13] R. K. Khadanga, A. Kumar, and S. Panda, "A modified grey wolf optimization with cuckoo search algorithm for load frequency controller design of hybrid power system," Appl. Soft Comput., vol. 124, p. 109011, 2022, doi: 10.1016/j.asoc.2022.109011.

[14] R. K. Khadanga, A. Kumar, and S. Panda, "A novel modified whale optimization algorithm for load frequency controller design of a two-area power system composing of PV grid and thermal generator," Neural Comput. Appl., vol. 32, no. 12, pp. 8205–8216, Jun. 2019, doi: 10.1007/s00521-019-04321-7.

[15] U. Dev et al., "Seasonal and Altitudinal Wind Energy Potential Assessment at Varying Heights UsingStochastic Modeling Approaches," AIUB Journal of Science and Engineering (AJSE), vol. 24, no. 3, p. 238, Jul. 2026, doi: 10.53799/k8y06q73.

[16] F. Kong et al., "Multi-area load frequency control of hydro-thermal-wind power based on improved grey wolf optimization algorithm," Elektron. Elektrotech., vol. 26, no. 6, pp. 32–39, Dec. 2020, doi: 10.5755/j01.eie.26.6.27484.

[17] X. Liang et al., "Chaotic oppositional sine–cosine method for solving global optimization problems," Eng. Comput., vol. 38, no. 2, pp. 1223–1239, Jul. 2020, doi: 10.1007/s00366-020-01083-y.

[18] S. Barshandeh and M. Haghzadeh, "A new hybrid chaotic atom search optimization based on tree-seed algorithm and Levy flight for solving optimization problems," Eng. Comput., vol. 37, no. 4, pp. 3079–3122, Feb. 2020, doi: 10.1007/s00366-020-00994-0.

[19] U. Dev et al., "Day Ahead Wind Energy Forecasting in Two Distinct Locations of Bangladesh Using Deep Learning Models," 2025 International Conference on Electrical, Computer and Communication Engineering (ECCE), Chittagong, Bangladesh, 2025, pp. 1-6, doi: 10.1109/ECCE64574.2025.11013432.

[20] S. Ozumcan, A. Ozturk, M. Varan, and C. Andic, "A novel honey badger algorithm-based load frequency controller design of a two-area system with renewable energy sources," Energy Rep., vol. 9, pp. 272–279, Oct. 2023, doi: 10.1016/j.egyr.2023.10.002.

[21] K. Balu and V. Mukherjee, "A novel quasi-oppositional chaotic Harris hawk's optimization algorithm for optimal siting and sizing of distributed generation in radial distribution system," Neural Process. Lett., vol. 54, no. 5, pp. 4051–4121, Apr. 2022, doi: 10.1007/s11063-022-10800-1.

[22] A. R. Sagor et al., "Osprey optimization algorithm for load frequency control in renewable and non-renewable energy based three-area power generating system," in Proc. Int. Conf. Robot., Electr. Signal Process. Technol. (ICREST), Dhaka, Bangladesh, 2025, pp. 465–470, doi: 10.1109/ICREST63960.2025.10914392.

[23] U. Dev et al., "Edge cutting and AI-driven protection strategies for DC microgrids: A comprehensive survey of challenges, technologies, and future trends," Results in Engineering, vol. 30, p. 110013, Mar. 2026, doi: 10.1016/j.rineng.2026.110013.

Sazzad Hossain Sahed is currently serving as a Graduate Teaching Assistant in the Faculty of Engineering at American International University-Bangladesh (AIUB) where he is pursuing his Master of Science (M.Sc.) in the Department of Electrical and Electronic Engineering. He received his Bachelor of Science (B.Sc.) in the Department of Electrical and Electronic Engineering from AIUB in 2023 with high distinction graduating with a CGPA of 3.98. Besides, he has an acute interest in English language which lead to his IELTS instructing journey having secured a band 8.0 in 2023. His field of interest revolves around power systems analysis, feasibility analysis of renewable energy, power transmission and distribution, controller manipulation and semiconductor materials.

Kazi Firoz Ahmed is a Ph.D. scholar at the Islamic University of Technology (IUT). He is doing his Ph.D. in the field of Power System Optimization. Currently, he is working as an Associate Professor at the EEE Department of American International University-Bangladesh (AIUB). He has been teaching and doing research at this university since 2010. He is the author of multiple published articles in journals and conference proceedings. Mr. Ahmed was a recipient of the OIC Scholarship from the Islamic University of Technology (IUT) for Excellence while doing his bachelor's.

Dr. Md. Rifat Hazari received his B.Sc. and M.Sc. degrees in Electrical and Electronic Engineering from the American International University-Bangladesh (AIUB) in August 2013 and December 2014, respectively and Ph.D. degree in Energy Engineering from the Kitami Institute of Technology (KIT), Japan, in March 2019. He has held various academic and administrative positions at AIUB, including Senior Assistant Professor, Assistant Professor and Lecturer in the Department of Electrical and Electronic Engineering (EEE), and Deputy Director of the Dr. Anwarul Abedin Institute of Innovation, AIUB. He is currently serving as an Associate Professor and Special Assistant in the EEE Department at AIUB. He has served as a Co-Principal Investigator (Co-PI) on multiple internationally funded research projects and has authored over 75 publications in peer-reviewed journals and national and international conferences.